Polarization and depolarization in scattering of cavity polaritons

Tomas Ostatnicky,[1] Dean Read,[1] and Alexey V. Kavokin[1,2]
[1]*School of Physics and Astronomy, University of Southampton, Highfield, Southampton SO17 1BJ, United Kingdom*
[2]*Dipartimento di Fisica, Universita di Roma II, 1 via della Ricerca Scientifica, Roma 00133, Italy*
(Received 28 January 2009; revised manuscript received 15 August 2009; published 29 September 2009)

We consider theoretically the elastic scattering of two exciton polaritons having opposite wave vectors in a planar microcavity. We derive the scattering amplitudes accounting for the vector polarization of polaritons and the interference of different scattering channels. We obtain a nontrivial dependence of the scattering amplitudes and the polarizations on the scattering angle and polarization of initial states. Generation of polariton spin currents as a result of scattering of linearly polarized polaritons is predicted. We also describe depolarization of exciton polaritons due to their scattering and show that it may be complete in certain scattering directions. This analysis provides a basis for engineering of spin- and electric field-sensitive optical logic gates based on exciton polaritons.

DOI: 10.1103/PhysRevB.80.115328 PACS number(s): 71.36.+c, 42.65.−k, 03.67.Mn

I. INTRODUCTION

Exciton polaritons in microcavities are composite bosons, which efficiently scatter each other due to multiple channels of direct and exchange Coulomb interaction of their constituent electrons and holes.[1–3] In the strong coupling regime, the exciton polaritons in microcavities are characterized by two dispersion branches split typically by several meV. Due to a strongly nonparabolic dispersion of the lower-polariton branch, various configurations for the resonant polariton-polariton scattering are possible.[2] The resonant scattering processes are responsible for the operations of the microcavity-based optical parametric oscillators (OPO).[4–6] Among various geometries of the polariton-based OPO studied until now, one of the most attractive implies scattering of two exciton polaritons having equal energies and opposite in-plane wave vectors on a so-called elastic circle [e.g., a circle in a two-dimensional (2D) reciprocal space characterized by some fixed value of the kinetic energy for the exciton polaritons,[7] see Fig. 1]. The advantage of this configuration is in the fully symmetric final quantum states (referred to as the signal and idler states), which is favorable for realization of the parametric oscillations.[8] The signal and idler states are characterized by the same polariton lifetime, which is not the case in the most popular microcavity OPO geometry based on the excitation of polaritons at the so called "magic angle" and their subsequent scattering to the lower and upper energy states.[4,5] On the other hand, the excitation geometry, which involves simultaneous generation of polaritons with opposite in-plane wave vectors, is more complex and harder to model due to the multitude of possible final states, as the scattering to any pair of states belonging to the same diameter of the elastic circle is allowed by the energy and wave vector conservation laws. Surprisingly, recent experimental studies revealed a strong angular dependence of the scattering probability on the polar angle. Moreover, they demonstrated the polarization selection rules in polariton-polariton scattering, which provided grounds for realization of the all-optical XNOR gates9 (i.e., gates which implement logical XNOR operation on polarized light beams).[9]

The experimental data of Ref. 9 has been interpreted using the spin-dependent Gross-Pitaevskii (GP) equations, which assume a single fully coherent polariton state characterized by a spinor wave function analogous to the classical Jones vector. Although a powerful and insightful method of modeling, the GP equations have two important shortcomings. First, they do not account for the possible depolarization of the polaritons during their scattering; second, they imply a contact interaction between the polaritons which is independent of their wave vectors. Here, we present a theoretical model, which relaxes the two above restrictions of the GP equations and allows for the description of a full range of polarization-dependent effects in polariton-polariton scattering, including depolarization. When applied to the specific scattering geometry of the experiment,[9] our formalism allows for the prediction of a nontrivial angular polarization dependence of the amplitude of polariton-polariton scattering and sheds light on the mechanisms of polarization relaxation in the polariton gases.

The spin-dependent Boltzmann equations describing the scattering of exciton polaritons with acoustic phonons and the polariton-polariton scattering have been formulated in Ref. 10, which treats the polariton spin dynamics within the Born-Markov approximation. Here, we extend the model of Ref. 10 accounting for the variations of the polariton-polariton scattering amplitudes with the vector of exchanged

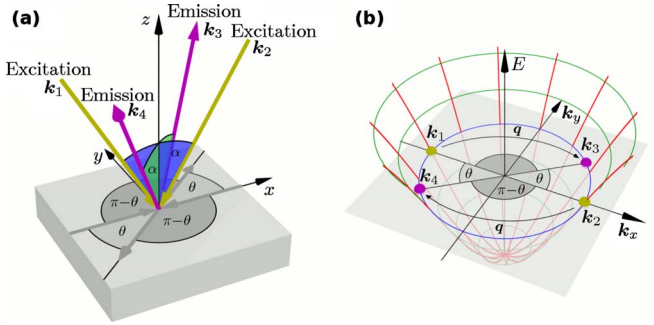

FIG. 1. (Color online) (a) Considered geometry of polariton-polariton scattering in real space with α being the angle of incidence and θ being the scattering angle. (b) In the reciprocal space, the dispersion of the lower-polariton branch is shown and the elastic circle is highlighted by the blue color.

momentum, which appears to be very important in the specific OPO geometry we consider. Moreover, we numerically evaluate the scattering amplitudes using a microscopic model which enables us to analyze the polariton pseudospin distributions on the elastic circle for different pump polarizations.

Introduction of the scattering amplitudes angular dependence in the model leads to appearance of new terms in the Boltzmann equations for the pseudospin components. These terms are responsible for the occurrence of new, interesting spin-related phenomena neglected so far, in particular, appearance of the circular polarization as a result of scattering of two linearly polarized polaritons and vice versa. In order to reveal the impact of these terms, we assume that the final states for polariton-polariton scattering are initially empty. This allows us to neglect stimulation of polariton-polariton scattering and consider only the spontaneous processes. We therefore use the density matrix formalism and a powerful algebraic analysis rather than the full (Boltzmann) rate equations given in Ref. 10. This approach enables us to formulate simple and universal polarization selection rules for polariton-polariton scattering.

The rest of this paper is organized as follows: Section II presents our model and polarization selection rules, Sec. III presents the numerical results for polariton pseudospin distributions, Sec. IV contains the conclusive remarks.

II. THEORETICAL MODEL

A. Scattering Hamiltonian

We consider a planar semiconductor microcavity in the strong exciton-light coupling regime. The cavity is pumped by two cw laser beams, which produce macroscopic populations of two cavity modes with opposite in-plane wave vectors $\boldsymbol{k}_1$ and $\boldsymbol{k}_2=-\boldsymbol{k}_1$. The angle of incidence of the two laser beams is the same (angle α in Fig. 1(a)). The polaritons scatter from the pump states to the final states obeying the momentum and energy conservation rule. In the configuration we consider, the pair interactions may scatter polaritons only to the states on the elastic circle defined by the in-plane momentum $|\boldsymbol{k}|=|\boldsymbol{k}_1|=|\boldsymbol{k}_2|$. These allowed final states are then fully identified by the scattering angle θ [Figs. 1(a) and 1(b)]. We shall consider the spontaneous polariton polariton scattering from the macroscopically populated pump states to the empty final states. We neglect depletion of the pump states due to the scattering and the longitudinal-transverse splitting (TE-TM splitting) of the exciton-polariton eigenstates is taken to be zero.

As pointed out in many publications,[11–14] excitons are not ideal bosons due to the fermionic nature of their constituents (electrons and holes). This is why also the cavity polaritons show some fermionic properties. The fermionic effects are negligible in the low-density limit, but they become important as soon as polariton-polariton interactions start playing a role. Strictly speaking, polariton-polariton scattering needs to be considered as a result of interactions of four fermions.[3,11,13] It is, however, possible and convenient to use an effective scattering Hamiltonian for the polaritons having the total angular momenta $s=\pm 1$ (which are strongly coupled to the optical field of the cavity mode). Using the above assumptions, one can easily see that such an effective Hamiltonian would couple the states on the elastic circle only to the pump states $\boldsymbol{k}_1$ and $\boldsymbol{k}_2$:

$$H_{\mathrm{SC}}=\frac{1}{2}\sum_{s,\boldsymbol{q}}\left[V_1(\boldsymbol{k}_1,\boldsymbol{k}_2,\boldsymbol{q})a^{+}_{s,\boldsymbol{k}_1+\boldsymbol{q}}a^{+}_{s,\boldsymbol{k}_2-\boldsymbol{q}}a_{s,\boldsymbol{k}_1}a_{s,\boldsymbol{k}_2}+V_2(\boldsymbol{k}_1,\boldsymbol{k}_2,\boldsymbol{q})a^{+}_{s,\boldsymbol{k}_1+\boldsymbol{q}}a^{+}_{-s,\boldsymbol{k}_2-\boldsymbol{q}}a_{s,\boldsymbol{k}_1}a_{-s,\boldsymbol{k}_2}\right]. \quad (1)$$

Here, $a_{s,\boldsymbol{k}}$ is the annihilation operator for a polariton having a wave vector $\boldsymbol{k}$ and spin s (the band index is omitted here since we consider only polaritons from the lower dispersion branch). The amplitudes V_1 and V_2 describe scattering of the polaritons with parallel and antiparallel spins. In general, $V_1\neq V_2$, as we shall discuss below in detail. The spin dependence of polariton-polariton interactions is at the origin of many peculiar effects in the polarization dynamics of exciton polaritons,[10,15] including the self-induced Larmor precession,[16] the rotation of linear polarization due to polariton-polariton scattering[17] and the buildup of linear polarization of the Bose-Einstein condensates of exciton-polaritons.[18]

Considering the scattering on the elastic circle, we define the wave vectors $\boldsymbol{k}_3(\theta)$ and $\boldsymbol{k}_4(\theta)$ of the scattered polaritons according to Fig. 1 (the argument will not be explicitly mentioned from now on) and present the exchanged momenta $\boldsymbol{q}=\boldsymbol{k}_3-\boldsymbol{k}_1$ and $\boldsymbol{q}'=\boldsymbol{k}_4-\boldsymbol{k}_1$. The Hamiltonian (1) then reads:

$$H_{\mathrm{SC}}=\sum_{s,\theta}\left(\beta_1(\theta)a^{+}_{s,\boldsymbol{k}_3}a^{+}_{s,\boldsymbol{k}_4}a_{s,\boldsymbol{k}_1}a_{s,\boldsymbol{k}_2}+\left[\beta_2(\theta)a^{+}_{s,\boldsymbol{k}_1+\boldsymbol{q}}a^{+}_{-s,\boldsymbol{k}_2-\boldsymbol{q}}+\beta_2'(\theta)a^{+}_{-s,\boldsymbol{k}_1+\boldsymbol{q}}a^{+}_{s,\boldsymbol{k}_2-\boldsymbol{q}}\right]a_{s,\boldsymbol{k}_1}a_{-s,\boldsymbol{k}_2}\right), \quad (2)$$

where the summation over the angle θ goes from 0 to π and we have defined more convenient scattering amplitudes (omitting the initial momenta in the arguments for clarity):

$$\beta_1(\theta)=\frac{1}{2}[V_1(\boldsymbol{q})+V_1(\boldsymbol{q}')], \quad (3)$$

$$\beta_2(\theta)=\frac{1}{2}V_2(\boldsymbol{q}), \quad (4)$$

$$\beta_2'(\theta)=\frac{1}{2}V_2(\boldsymbol{q}')=\beta_2(\pi-\theta). \quad (5)$$

The matrix elements of the Hamiltonian (2) for selected spins of the initial and final states are shown in Table I. They should be interpreted carefully: the nonzero matrix element $\langle XX|H_{\mathrm{SC}}|XX\rangle$ (where the bra and ket vectors denote the final and initial spin states, respectively) expresses only the fact that in the case of excitation by two X-polarized beams, the conditional probability of finding the X-polarized polariton in the direction $\boldsymbol{k}_3$ when we observe another X-polarized polariton in the direction $\boldsymbol{k}_4$ is nonzero (and proportional to the matrix element squared). It does not mean, however, that the final states are X polarized because also the matrix element $\langle YY|H_{\mathrm{SC}}|XX\rangle$ is nonzero and a Y-polarized component in the emission is expected to appear as well. Surprisingly, the emission will not be polarized at all if $\beta_2=\beta_2'=0$ or $\beta_1=0$ because both the aforementioned matrix elements have the same magnitude and the probability of scattering to the states $|XX\rangle$ and $|YY\rangle$ is equal. We then find that the final states are in a non–polarized entangled state $(|XX\rangle+|YY\rangle)/\sqrt{2}$.

TABLE I. Matrix elements of the Hamiltonian (3) for selected spin combinations of the incoming and outgoing polaritons. Polarization state $L(\varphi)$ is defined as the linear polarization rotated by an angle φ with respect to the X-polarized state and we define $\varepsilon=\exp[-i\varphi]$. The notation in the table is as follows: $\sigma^+\sigma^-$ for the initial state denotes the $s=1$ polariton in the state $\boldsymbol{k}_1$ and $s=-1$ polariton in the state $\boldsymbol{k}_2$. Same for the final states. The matrix element for the $\sigma^-\sigma^+$ configuration may be retrieved by permutation of β_2 and β_2'.

	Final state						
Initial state	$\sigma^+\sigma^+$	$\sigma^+\sigma^-$	$\sigma^-\sigma^-$	XX	XY	YY	$XL(\varphi)$
$\sigma^+\sigma^+$	β_1	0	0	$\beta_1/2$	$i\beta_1/2$	$-\beta_1/2$	$\varepsilon^*\beta_1/2$
$\sigma^+\sigma^-$	0	β_2	0	$(\beta_2+\beta_2')/2$	$-i(\beta_2-\beta_2')/2$	$(\beta_2+\beta_2')/2$	$(\varepsilon\beta_2+\varepsilon^*\beta_2')/2$
$\sigma^-\sigma^-$	0	0	β_1	$\beta_1/2$	$-i\beta_1/2$	$-\beta_1/2$	$\varepsilon\beta_1/2$
XX	$\beta_1/2$	$(\beta_2+\beta_2')/2$	$\beta_1/2$	$(\beta_1+\beta_2+\beta_2')/2$	0	$(\beta_2+\beta_2'-\beta_1)/2$	$(\beta_1+\beta_2+\beta_2')\cdot(\cos\varphi)/2$
XY	$-i\beta_1/2$	$i(\beta_2-\beta_2')/2$	$i\beta_1/2$	0	$(\beta_1+\beta_2-\beta_2')/2$	0	$(\beta_1+\beta_2-\beta_2')\cdot(\sin\varphi)/2$
YY	$-\beta_1/2$	$(\beta_2+\beta_2')/2$	$-\beta_1/2$	$(\beta_2+\beta_2'-\beta_1)/2$	0	$(\beta_1+\beta_2+\beta_2')/2$	$(\beta_2+\beta_2'-\beta_1)\cdot(\cos\varphi)/2$

B. Scattering amplitudes

In order to quantitatively characterize the emission from a microcavity in the limit of spontaneous scattering on the elastic circle, we shall evaluate or estimate the amplitudes of the coefficients β_1, β_2, and β_2'. One can expand:

$$V_1(\mathbf{q},\mathbf{k}_1,\mathbf{k}_2)|X_H|^{-4} = V_{\text{dir}}(\mathbf{q},\mathbf{k}_1,\mathbf{k}_2) + V_{\text{exch}}(\mathbf{q},\mathbf{k}_1,\mathbf{k}_2), \quad (6)$$

$$V_2(\mathbf{q},\mathbf{k}_1,\mathbf{k}_2)|X_H|^{-4} = V_{\text{dir}}(\mathbf{q},\mathbf{k}_1,\mathbf{k}_2) + V_{\text{super}}. \quad (7)$$

The beta coefficients are then retrieved following the definitions (3)–(5). X_H denotes the Hopfield coefficient describing the excitonic fraction of polariton states at the elastic circle. In Eqs. (6) and (7), the scattering amplitudes were decomposed[11,14] into the exciton direct-scattering part V_{dir} and the exchange-scattering parts V_{exch}, V_{super}. The part V_{super} is an effective exchange contribution originating in higher-order processes, which involve virtual excitation of the optically forbidden exciton states with spins ± 2 (superexchange). Scattering between the optically active polariton states and the dark excitons has been addressed in detail in Refs. 19–21.

We performed numerical calculations of the direct scattering amplitude for exciton-polaritons on the elastic circle using the microscopic model.[22,23] We found that the scattering amplitudes do not depend on the particular orientation of the contributing wave vectors and thus we use the notation $q=|\boldsymbol{q}|$ and $k_j=|\boldsymbol{k}_j|$ in the following. We also carried out numerical calculations of the exchange term V_{exch}, which displayed a virtually constant behavior for small q. We therefore consider that both the exchange and the superexchange terms are constant around the elastic circle. Clearly, the characteristic scale on which these terms might change is given by the inverse exciton Bohr radius a_B^{-1}, which is orders of magnitude larger than the radius of the elastic circle which we consider.

The direct term, on the contrary, reveals a strong dependence on the exchanged momentum for $q \ll a_B^{-1}$, according to Refs. 22 and 23, and provides zero scattering amplitude for $q=0$ in the 2D exciton gas limit. The scattering amplitude varies as $(qa_B)^3$ and is estimated as $V_{\text{dir}}(0.1a_B^{-1})/V_{\text{exch}} \approx 1.5\cdot 10^{-4}$ giving only a negligible contribution to the overall scattering amplitudes in Eqs. (6) and (7). The small amplitude of the direct term is, nevertheless, caused by compensation of the electron-electron and hole-hole repulsion by electron-hole attraction, and the direct term completely vanishes if the effective masses of the fermions become equal. The different shape of the electron and the hole wave functions in realistic quantum wells (QWs) cause the nonzero amplitude of the direct Coulomb interaction. We show here that this direct term may become orders of magnitude larger in narrow QWs compared to the ideal 2D exciton gas because of the wave function penetration into the barriers (for the discussion of the effect of charge separation see Ref. 14).

We derived an analytical expression for the direct scattering term amplitude considering a real exciton wave function in a narrow QW in the integral form (see Appendix) and then evaluated it numerically. The effect of charge separation on the amplitude of the direct term is obvious from Eq. (A3): the larger difference between the square of the electron and hole wave function is, the larger value of the scattering amplitude. In real, narrow GaAs QWs, coincidentally, the ratio between the electron and the hole mass is about 1/6, which is why electrons deeply penetrate into the QW barriers when the hole are kept localized in the QW layer. The effect of delocalization is even more pronounced in QWs with low-band offsets, e.g., InGaAs/GaAs with low In content. The amplitude of the direct term therefore strongly depends on the QW width and composition.

We plot the direct term amplitude in the units of the exchange interaction amplitude in Fig. 2(a) for the frequently used GaAs/$Al_{0.3}Ga_{0.7}As$ and $In_{0.04}Ga_{0.96}As$/GaAs QWs of the widths 2.5 and 5 nm, respectively. The electron wave function spreading into narrow QW barriers causes the significant increase of the direct scattering amplitude, which now has a nonzero value at zero exchanged momentum [the particular wave functions are plotted in the inset of Fig. 2(b)]. When inspecting the angular dependence of the spin and intensity of the scattered signal on the elastic circle, not only the offset but also the absolute value of the amplitude variations with the exchanged momentum are important. In this case, the variations are larger by over two orders of magnitude in the case of the $In_{0.04}Ga_{0.96}As$/GaAs QW, as compared to the GaAs/$Al_{0.3}Ga_{0.7}As$ QW, in the range of wave vectors up to 2 μm^{-1}.

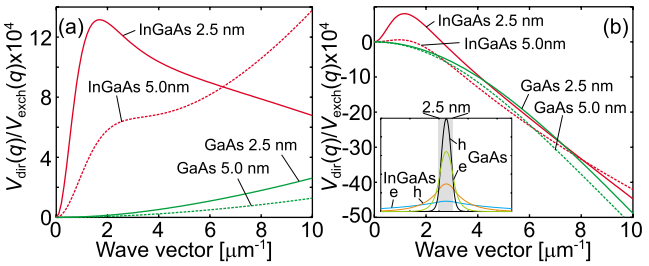

FIG. 2. (Color online) Ratio between the direct and exchange-scattering amplitude considering zero (a) and nonzero (b) applied voltage perpendicular to the QW plane for real QWs. Nonzero voltage is assumed to induce spatial shift of each of the particle wave functions by 1 nm in opposite directions. Different QW compositions and widths are taken into account. The curve offsets were removed for clarity, their values are: (a) InGaAs 2.5 nm: 0.22, InGaAs 5 nm: 0.089, GaAs 2.5 nm: 0.007, GaAs 5 nm: 0.002, (b) InGaAs 2.5 nm: 0.27, InGaAs 5 nm: 0.17, GaAs 2.5 nm: 0.30, GaAs 5 nm: 0.24. Inset: calculated electron (e) and hole (h) wave functions squared in 2.5 nm wide QW for the two GaAs/AlGaAs and InGaAs/GaAs compositions.

A further electron-hole separation may be induced by applying an electric field in normal to the QW plane direction. Although the exciton oscillator strength may be reduced in this case due to the quantum confined Stark effect, the system may be kept in the strong coupling regime if the Q factor of the cavity is high enough. In this case, the direct term and its variation along the elastic circle are further increased as one can see from Fig. 2(b), where we plot the amplitude of the direct term for the InGaAs/GaAs and GaAs/AlGaAs QWs considering the electron and the hole centers of mass spatially separated by 1 nm. The difference between the scattering amplitudes in the two types of III-V QWs we considered almost vanishes at strong applied bias.

To estimate the magnitude of external electric field needed for the efficient charge separation, let us consider a plane capacitor formed by two plates electrically charged with the density ρ. Considering the QW excitons, the charge density may be estimated as $\rho=e(1-S)/\pi a_B^2$, where S is the electron-hole overlap integral, e is the electron charge and a_B is the exciton Bohr radius. The electric field created by one of the planes and acting upon another one is independent on the distance between them, $E_P=\rho/2\varepsilon$ where ε is static dielectric constant. The electron-hole system is in equilibrium if the field E_P is compensated by an external field of the same magnitude. This allows estimating of the external field as $E=\frac{e}{2\pi\varepsilon}\frac{1-S}{a_B^2}$. Substituting $\varepsilon_r=10$ and the Bohr radius $a_B=10$ nm, we obtain $E\approx(1-S)\cdot 30$ kV/cm. The reduction of the electron-hole overlap S due to the spatial separation of electron and hole centers of mass by 1 nm is, approximately, 30% and 50% in 5 and 2.5 nm wide InGaAs/GaAs QWs, respectively, and 55% and 85% in 5 and 2.5 nm wide GaAs/AlGaAs QWs, respectively. These numbers imply the required external electric field intensities in the range 10–25 kV/cm, depending on the QW composition and width. These values are in a good agreement with the results of Ref. 24, which gives an estimate of the same order for CdTe/CdZnTe QWs.

Finally, the magnitude of the superexchange scattering channel may be estimated from the T-matrix calculations published in Refs. 20 and 21. We use the ratio $V_{super}/V_{exch}=T^{+-}/T^{++}=-0.28+0.01i$ for all QWs under consideration.

C. Spin and polarization of the final states

As pointed out above, the Hamiltonian (2) and its matrix elements in Table I do not directly show either the degree of polarization or the polarization of the final states themselves. We therefore develop an algebraic procedure for calculation of both these quantities from the Hamiltonian (2). The system of interacting polaritons is described by the density matrix $\rho(t)$ with an initial condition $\rho(t=0)=\rho_0$. We assume that the dephasing in the system is strong due to interactions between polaritons and phonons what allows one to use the Born-Markov approximation[10] for evaluation of the density matrix dynamics. This procedure yields:

$$\frac{d\rho(t)}{dt}=-\frac{2\pi}{\hbar^2}\delta(E_f-E_i)\{H_{SC},[H_{SC},\rho(t)]\}, \tag{8}$$

where $E_{f,i}$ are the energies of the final and the initial state, respectively, and the Dirac delta function is responsible for energy conservation. As we discussed above, the final states are weakly populated and therefore the system response in an arbitrary scattering direction is governed only by the populations of the initial states and the scattering angle θ (i.e., no stimulated scattering). This assumption allows us to substitute $\rho(t)=\rho_0$ in the right hand side of Eq. (8). It is also obvious that we do not need to know the evolution of the whole density matrix, which is why we fragment it to the submatrices whose evolution is of particular interest.

We define the 2×2 spin-density matrix $\rho_{\boldsymbol{k}}$ for a state with a wave vector $\boldsymbol{k}$ in the basis of spins $\{\sigma^+,\sigma^-\}$. The 4×4 joint density matrix for the final states is therefore defined as a direct product $\rho_{\boldsymbol{k}_3(\theta),\boldsymbol{k}_4(\theta)}=\rho_{\boldsymbol{k}_3(\theta)}\otimes\rho_{\boldsymbol{k}_4(\theta)}$ and it fully describes the spin states of the scattered polaritons. The equation of motion for this density matrix can be straightforwardly derived from Eq. (8) within the assumptions made:

$$\frac{d\rho_{\boldsymbol{k}_3(\theta),\boldsymbol{k}_4(\theta)}(t)}{dt}=-\frac{4\pi}{\hbar^2}\delta(E_f-E_i)H_B^+(\theta)\rho_{\boldsymbol{k}_1,\boldsymbol{k}_2}H_B(\theta), \tag{9}$$

where the joint density matrix for the initial states is $\rho_{\mathbf{k}_1,\mathbf{k}_2}=\rho_{\mathbf{k}_1}\otimes\rho_{\mathbf{k}_2}$ and the Hamiltonian sub-block H_B reads:

$$H_B(\theta)=\begin{pmatrix}\beta_1(\theta) & 0 & 0 & 0\\ 0 & \beta_2(\theta) & \beta_2'(\theta) & 0\\ 0 & \beta_2'(\theta) & \beta_2(\theta) & 0\\ 0 & 0 & 0 & \beta_1(\theta)\end{pmatrix}. \tag{10}$$

We are interested in the polarization of the radiation emerging in some definite direction denoted by the wave-vector $\boldsymbol{k}_3$ (see Fig. 1). The polarization properties of the radiation are fully described by the pseudospin vector $\boldsymbol{S}_{\boldsymbol{k}_3}$. We define the spin matrix in the usual way[10] $\rho_{\boldsymbol{k}_3}=\frac{1}{2}N_{\boldsymbol{k}_3}+\boldsymbol{S}_{\boldsymbol{k}_3}\cdot\boldsymbol{\sigma}$, where $N_{\boldsymbol{k}_3}$ is the polariton population in the direction $\boldsymbol{k}_3$ and $\boldsymbol{\sigma}$ is the vector of Pauli matrices. The population and pseudospin components of the final state may be retrieved by evaluation

of appropriate quantum-mechanical mean values:

$$N_{\boldsymbol{k}_3}(t) = \sum_s \langle a^+_{s,\boldsymbol{k}_3} a_{s,\boldsymbol{k}_3} \rangle = \mathrm{Tr}[(\boldsymbol{I}\otimes\boldsymbol{I})\rho_{\boldsymbol{k}_{3(\theta)},\boldsymbol{k}_{4(\theta)}}(t)], \quad (11)$$

$$S_{x,\boldsymbol{k}_3}(t) = \frac{1}{2}\sum_s \langle a^+_{s,\boldsymbol{k}_3} a_{-s,\boldsymbol{k}_3} \rangle = \frac{1}{2}\mathrm{Tr}[(\boldsymbol{\sigma}_x\otimes\boldsymbol{I})\rho_{\boldsymbol{k}_{3(\theta)},\boldsymbol{k}_{4(\theta)}}(t)], \quad (12)$$

$$S_{y,\boldsymbol{k}_3}(t) = \frac{\mathrm{i}}{2}\sum_s s\langle a^+_{s,\boldsymbol{k}_3} a_{-s,\boldsymbol{k}_3} \rangle = \frac{1}{2}\mathrm{Tr}[(\boldsymbol{\sigma}_y\otimes\boldsymbol{I})\rho_{\boldsymbol{k}_{3(\theta)},\boldsymbol{k}_{4(\theta)}}(t)], \quad (13)$$

$$S_{z,\boldsymbol{k}_3}(t) = \frac{1}{2}\sum_s s\langle a^+_{s,\boldsymbol{k}_3} a_{s,\boldsymbol{k}_3} \rangle = \frac{1}{2}\mathrm{Tr}[(\boldsymbol{\sigma}_z\otimes\boldsymbol{I})\rho_{\boldsymbol{k}_{3(\theta)},\boldsymbol{k}_{4(\theta)}}(t)]. \quad (14)$$

The symbol $\boldsymbol{I}$ denotes here the 2×2 unit matrix. Considering finite lifetime of polaritons τ and cw excitation, the steady-state pseudospin components may be derived as $S_j^{\mathrm{steady}} = \tau[\mathrm{d}S_j/\mathrm{d}t]_{\mathrm{coh}}$, where the "coh" index denotes the coherent temporal evolution according to Eq. (9). Using Eqs. (9) and (11)–(14), we obtain the steady-state pseudospin components:

$$N_3^{\mathrm{steady}} \propto (\beta_1^2 + |\beta_2|^2 + |\beta_2'|^2)N_1N_2 + 8\,\mathrm{Re}[\beta_2(\beta_2')^*]S_{1x}S_{2x} + 8\,\mathrm{Re}[\beta_2^*\beta_2']S_{1y}S_{2y} + 4(\beta_1^2 - |\beta_2|^2 - |\beta_2'|^2)S_{1z}S_{2z}, \quad (15)$$

$$S_{3x}^{\mathrm{steady}} \propto 2\beta_1\,\mathrm{Re}(\beta_2')S_{1x}N_2 + 2\beta_1\,\mathrm{Re}(\beta_2)N_1S_{2x} + 4\beta_1\,\mathrm{Im}(\beta_2)S_{1z}S_{2y} + 4\beta_1\,\mathrm{Im}(\beta_2')S_{1y}S_{2z}, \quad (16)$$

$$S_{3y}^{\mathrm{steady}} \propto 2\beta_1\,\mathrm{Re}(\beta_2')S_{1y}N_2 + 2\beta_1\,\mathrm{Re}(\beta_2)N_1S_{2y} - 4\beta_1\,\mathrm{Im}(\beta_2)S_{1z}S_{2x} - 4\beta_1\,\mathrm{Im}(\beta_2')S_{1x}S_{2z}, \quad (17)$$

$$S_{3z}^{\mathrm{steady}} \propto (\beta_1^2 - |\beta_2|^2 + |\beta_2'|^2)S_{1z}N_2 + (\beta_1^2 + |\beta_2|^2 - |\beta_2'|^2)N_1S_{2z} + 4\,\mathrm{Im}[\beta_2(\beta_2')^*]S_{1y}S_{2x} + 4\,\mathrm{Im}[\beta_2^*\beta_2']S_{1x}S_{2y}. \quad (18)$$

Compared to Ref. 10, we obtained several new terms in the kinetic equations for the pseudospin components. The origin and the role of these terms are discussed in the next Section.

III. RESULTS AND DISCUSSION

A. Polarization selction rules

Here, we consider the polarization selection rules which govern polariton-polariton scattering on the elastic circle. The final state polarizations are analyzed as a function of the scattering angle. The angle dependence of the scattering amplitudes comes from the direct Coulomb scattering term, while the exchange and superexchange contributions are virtually insensitive to the scattering angle if the radius of the elastic circle is much less than the inverse exciton Bohr radius.

The total polarization degree of a polariton quantum state $\boldsymbol{k}_3$ can be defined as $P = 2|\boldsymbol{S}_3|/N_3$. Obviously, this quantity ranges between 0 (nonpolarized state) and 1 (fully polarized state). We note that Eqs. (16)–(18) account for the possible depolarization of the final states with respect to the initial states. For example, if considering fully colinearly polarized initial states, we obtain for the total polarization degree of the final states:

$$P = \frac{2|\beta_1\,\mathrm{Re}(\beta_2 + \beta_2')|}{\beta_1^2 + |\beta_2|^2 + |\beta_2'|^2 + 2\,\mathrm{Re}(\beta_2^*\beta_2')}. \quad (19)$$

P is zero if $\beta_2 = \beta_2' = 0$ or $\beta_1 = 0$ (cf. Table I and the discussion at the end of Sec. II A) and equals 1 if $\beta_2 = \beta_2' = \pm\beta_1/2$. The ratios β_2/β_1 and β_2'/β_1 determine the degree of polarization and also the orientation of the pseudospin vector. The exchange interaction couples the initial states with colinear polarizations to the final states with the parallel and perpendicular linear polarizations with the same probability (see Table I). This is why, in this configuration, only the superexchange term and the direct interaction term affect the polarization degree of the final states. The coefficients β_2 and β_2' may be negative if the exchanged momentum is small and therefore the inversion of linear polarization is often observed in the polariton-polariton scattering experiments.[16,17]

The effect of depolarization in polariton-polariton scattering has not been addressed theoretically so far, to the best of our knowledge. Here, we show that it is indeed a general feature of polariton-polariton scattering in the spontaneous regime. This effect limits accuracy of the Gross-Pitaevskii equations which assume full coherence and polarization in the system. On the other hand, the depolarization effect is likely to be reduced if the scattering of polaritons is stimulated by final state populations. In this regime, a selected polarization is likely to be amplified, so that the total polarization degree increases.

When compared to Ref. 10, we observe the new terms in Eqs. (16)–(18). These terms emerge from the fact that we consider the complex and angle-dependent scattering amplitude V_2 and therefore $\beta_2 \neq \beta_2'$ and $\mathrm{Im}\,\beta_2 \neq 0$ in general. Except for these differences, the results of Ref. 10 in the limit of spontaneous scattering are fully reproduced. Knowing the angular dependence of V_2 we are able to predict the dependence of the pseudospin components on the scattering angle.

Moreover, we find a new possibility of polarization conversion as a result of polariton-polariton scattering. In order to illustrate this, let us consider Eq. (18). The last two terms in it describe creation of the circular polarization component from two incoming polaritons with linear polarizations rotated by 45° with respect to each other. As the states on the elastic circle with nonzero wave vectors are created, this means creation of the spin currents with well defined propagation directions. We recall that polariton spin currents may be generated in microcavities due to the Optical Spin Hall effect[25,26] caused by the TE-TM splitting of exciton-polaritons and their elastic scattering by a static disorder potential. The effect we propose here does not require either disorder scattering, or TE-TM splitting but exploits the specific selection rules in the polariton-polariton scattering.

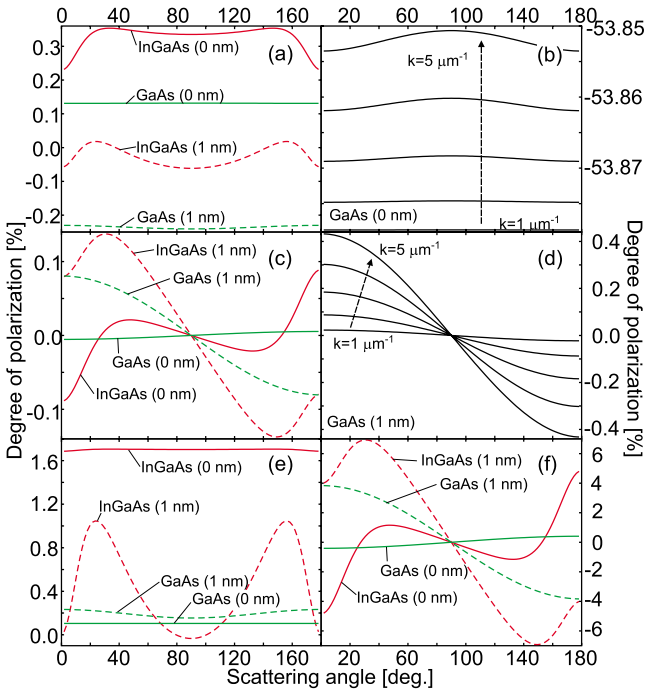

FIG. 3. (Color online) Linear polarization degree P_x in scattering of colinearly (a–b,e) and cross-linearly (c–d,f) polarized pump beams as a function of scattering angle. Spontaneous scattering only is considered in (a–d) while (e–f) display calculations with stimulation of the polariton scattering taken into account. We compare different QW compositions (a,c,e–f) (circle radius 2 μm^{-1}) and elastic circle radii for "GaAs (0 nm)" QW (b) and "GaAs (1 nm)" QW (d). The numbers in parentheses mean spatial shift of the particle wave functions due to the applied electric field. Curves in (a,e) have nonzero offsets which were removed for clarity: (a) GaAs (0 nm): −52%, GaAs (1 nm): +4%, InGaAs (0 nm): −11%, InGaAs (1 nm): −2%, (e) GaAs (0 nm): −100%, GaAs (1 nm): +60%, InGaAs (0 nm): −100%, InGaAs (1 nm): −35%. The QW width is always 2.5 nm.

Note that the total spin is conserved by the process we consider, because the build up of some degree of circular polarization in one direction is compensated by appearance of an opposite circular polarization degree in the opposite scattering direction. Equations (16) and (17) allow for an inverse process: the creation of linear polarization from one linearly and one circularly polarized initial state. This process is reflected by the elements of the rightmost column in Table I.

We note that the process described above is possible due to the existence of a nonzero imaginary part of the scattering amplitude V_2. The argument is that V_2 contains contributions in both first and second order of the perturbation theory (direct and superexchange terms, respectively), which bring different phases, so their sum is a complex number with nonzero real and imaginary parts.

B. Numerical simulations

The numerical solutions of Eqs. (16)–(18) are plotted in Figs. 3 and 4. Here we consider a microcavity with a 2.5 nm wide $In_{0.04}Ga_{0.96}As/GaAs$ or $GaAs/Al_{0.3}Ga_{0.7}As$ QW. We

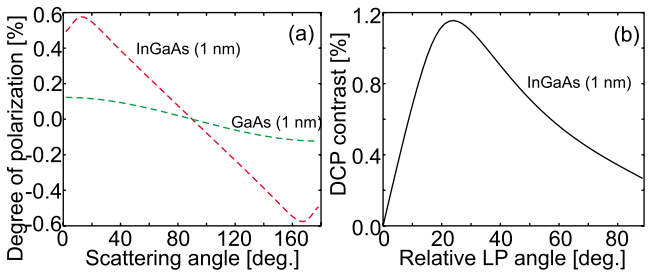

FIG. 4. (Color online) (a) Degree of circular polarization around the elastic circle for two different 2.5 nm wide QW compositions above the stimulated threshold. (b) Dependence of the degree of circular polarization (DCP) contrast on the elastic circle on the angle between vectors of linear polarization of the incident beams.

have fixed $V_{super}/V_{exch}=-0.28+0.01i$ following the results of Schumacher *et al.*[20,27]

The linear polarization degree of the final states defined as $P_x=2S_{3x}/N_3$ is plotted in Figs. 3(a)–3(d) in the case of colinear (X polarized) and cross-linear polarizations of the initial states, respectively, as a function of the scattering angle. The curves in Figs. 3(a) and 3(c) are calculated accounting for the electron and hole spatial separation due to an applied electric field for both types of QWs, Figs. 3(b) and 3(d) illustrates the wave vector dependence of the degree of polarization in the GaAs/AlGaAs QW.

We observe from Fig. 3(a) that the inversion of the linear polarization degree in the case of scattering of collinearly polarized polaritons takes place unless Re $\beta_2>0$. Without the strong direct Coulomb interaction, the linear polarization degree would be $P_x=2(V_{super}/V_{exch})/[1+(V_{super}/V_{exch})^2]\approx 52\%$ in the steady-state regime, however the direct interaction compensates the effect of the linear polarization rotation and the degree of linear polarization is expected to reach the value of only 11% in narrow InGaAs/GaAs QWs. The contrast of the degree of linear polarization around the elastic circle is of only a few tenths of per cent due to the nearly quadratic behavior of the direct term amplitude as a function of the exchanged wave vector [see Fig. 2(a)]. The contrast is increased if the wave vector of incident beams (elastic circle radius) is increased as shown in Fig. 3(b).

Figure 3(c) shows nontrivial variations of the degree of linear polarization as a function of the scattering angle if we consider excitation by cross-polarized beams (note that the X-polarized beam is incident at $\theta=180°$). The degree depends very strongly on the particular shapes of the electron and hole wave functions, and obviously the polarization of the emitted light may be controlled by the applied voltage. The dependence of the polarization degree on the elastic circle radius for a GaAs/AlGaAs QW subjected to the external bias is shown in Fig. 3(d). The elastic circle radius affects the value of the exchanged wave vector, which governs the final state polarizations.

The calculations presented in Figs. 3(a)–3(d) show only a weak variation of the linear polarization degree on the elastic circle (below one per cent). However, so far we have neglected the final state stimulation of the polariton-polariton scattering, which is expected to magnify the polarization variation. In order to reveal this effect, we have solved the

equations of motion for polariton pseudospin taking into account the stimulated processes in polariton–polariton scattering. The results are plotted in Figs. 3(e) and 3(f) for the same parameters as in Figs. 3(a) and 3(c). One can see that the polarization degree as well as its variations strongly increase. The variations may be as large as several per cent in this case. We also observe that depolarization takes place even in the stimulated regime (polarization degree is only 35% in InGaAs QW).

The buildup of the circular polarization and generation of polariton spin currents by linearly polarized optical pumps is demonstrated in Fig. 4. There the pumps have linear polarizations whose planes are rotated by 22° with respect to each other [at this angle the highest circular polarization degree is observed, see Fig. 4(b)]. In this calculation, we considered the stimulated scattering regime, in which case the circular polarization contrast exceeds one per cent. This effect, which may be cautiously referred to as the intrinsic optical spin Hall effect, is relatively weak in the model microcavities we have considered. On the other hand its magnitude depends on the spatial separation of electrons and holes in the QW growth direction so that it can be tuned by applying an external bias.

IV. CONCLUSIONS

We have analyzed the polarization selection rules for the elastic scattering of exciton polaritons in a semiconductor microcavity in the strong coupling regime. We show that the polarization of scattered polaritons may be different from the polarization of pumping light. In particular, linear polarization may be rotated by 90 degrees and circular polarization may be builtup from linearly polarized pumping. We show that when scattered in particular directions the polaritons lose their polarization and become unpolarized.

Using a microscopic model, we have calculated the scattering angle dependence of the polariton-polariton scattering amplitudes on the elastic circle. We have shown that the amplitude of the direct Coulomb scattering process is angle dependent and reveals the pronounced minima and maxima as one goes around the elastic circle. The angular dependence is more pronounced in QWs with spatially separated electron and hole centers of mass. This offers an opportunity to tune the final state polarization by the external electric field. On the other hand, the contributions from the exchange and superexchange polariton coupling mechanisms are virtually independent of the scattering angle. We have found terms previously neglected in the pseudospin kinetic equations arising from the wave vector dependence of the scattering amplitudes and their imaginary components. These terms are shown to be responsible for a variety of effects. We have demonstrated that polariton spin currents (circular polarization currents) may be generated using linearly polarized pump beams. This analysis provides a basis for engineering of spin-sensitive optical logic gates based on exciton polaritons.

The demonstrated sensitivity of the direct scattering term to the QW geometry and to the applied voltage offers the opportunity to control the polariton-polariton interactions and their spin selection rules via the microcavity design (e.g., introducing coupled QWs or superlattices) and external fields. We believe that the effects predicted in this paper may be used in future field-controlled spintronic devices.

ACKNOWLEDGMENTS

We acknowledge enlightening discussions with I. A. Shelykh, H. Ouerdane, and M. M. Glazov. We thank the EPSRC for financial support.

APPENDIX

The direct scattering term is given by the integral:[23]

$$V_{\mathrm{dir}} = \int \varphi_3^*(\boldsymbol{r}_1,\boldsymbol{r}_1')\varphi_4^*(\boldsymbol{r}_2,\boldsymbol{r}_2')V(\boldsymbol{r}_1,\boldsymbol{r}_1',\boldsymbol{r}_2,\mathbf{r}_2') \times \varphi_1(\boldsymbol{r}_1,\boldsymbol{r}_1')\varphi_2(\boldsymbol{r}_2,\boldsymbol{r}_2')\mathrm{d}\boldsymbol{r}_1 \ldots \boldsymbol{r}_2', \tag{A1}$$

where the nonprimed $\boldsymbol{r}$'s are the electron coordinates and the primed ones are the hole coordinates. Symbol V stands for the Coulomb potential and φ's are the initial and the final state wave functions with appropriate indices. Note that the vectors are three-dimensional. We factorize the wave functions as products of the in-plane and z-components as $\varphi_{\boldsymbol{k}}(\boldsymbol{r},\boldsymbol{r}')=N\mathrm{e}^{-i\boldsymbol{k}\cdot\boldsymbol{R}}\psi(\boldsymbol{\rho})\chi(z)\chi'(z')$ where N is the normalization constant, $\boldsymbol{k}$ is the in-plane wave vector, $\boldsymbol{R}$ is the center-of-mass coordinate, $\boldsymbol{\rho}$ is the relative electron-hole coordinate and χ and χ' are the respective wave functions of an electron and a hole in a QW. Considering $\psi(\boldsymbol{\rho})=\exp[-\rho/a_{\mathrm{B}}]$ and $|\boldsymbol{k}| \ll a_{\mathrm{B}}^{-1}$, we may do a straightforward evaluation, restricting only to the most important terms:

$$V_{\mathrm{dir}}(q) \approx \frac{e^2}{\varepsilon a_{\mathrm{B}}}\frac{a_{\mathrm{B}}^2}{S}\frac{\pi}{4a_{\mathrm{B}}q}\left\{\int [\chi^2(z_1)\chi^2(z_2)+\chi'^2(z_1)\chi'^2(z_2)-2\chi^2(z_1)\chi'^2(z_2)]f(q,z_1,z_2)\mathrm{d}z_{1,2}\right.$$
$$-\frac{3(qa_{\mathrm{B}})^2}{4}\int [\chi^2(z_1)\chi^2(z_2)\gamma'^2+\chi'^2(z_1)\chi'^2(z_2)\gamma^2-\chi^2(z_1)\chi'^2(z_2)(\gamma^2+\gamma'^2)]f(q,z_1,z_2)\mathrm{d}z_{1,2}$$
$$\left.-\frac{3(qa_{\mathrm{B}})^4}{64}\int [\chi^2(z_1)\chi^2(z_2)\gamma'^4+\chi'^2(z_1)\chi'^2(z_2)\gamma^4-2\chi^2(z_1)\chi'^2(z_2)(2(\gamma^4+\gamma'^4)-3\gamma^2\gamma'^2)]f(q,z_1,z_2)\mathrm{d}z_{1,2}\right\} \tag{A2}$$

$$f(q,z_1,z_2) = \int_0^\infty \frac{x}{\sqrt{x^2 + q^2(z_1 - z_2)^2}} J_0(x)\mathrm{d}x. \tag{A3}$$

Here, e stands for the electron charge, ε is the static dielectric constant, S is the normalization surface, J_0 is the Bessel function, γ and γ' are the respective electron and hole reduced masses. The exchanged wave vector is denoted by q.

[1] F. Tassone and Y. Yamamoto, Phys. Rev. B **59**, 10830 (1999).
[2] C. Ciuti, P. Schwendimann, B. Deveaud, and A. Quattropani, Phys. Rev. B **62**, R4825 (2000).
[3] M. Combescot, O. Betbeder-Matibet, and R. Combescot, Phys. Rev. Lett. **99**, 176403 (2007).
[4] R. M. Stevenson, V. N. Astratov, M. S. Skolnick, D. M. Whittaker, M. Emam-Ismail, A. I. Tartakovskii, P. G. Savvidis, J. J. Baumberg, and J. S. Roberts, Phys. Rev. Lett. **85**, 3680 (2000).
[5] M. Saba, C. Ciuti, J. Bloch, V. Thierry-Mieg, R. André, Le Si Dang, S. Kundermann, A. Mura, G. Bongiovanni, J. L. Staehli, and B. Deveaud, Nature (London) **414**, 731 (2001).
[6] C. Diederichs, J. Tignon, G. Dasbach, C. Ciuti, A. Lemaître, J. Bloch, P. Roussignol, C. Delalande, Nature (London) **440**, 904 (2006).
[7] W. Langbein and J. M. Hvam, Phys. Rev. Lett. **88**, 047401 (2002).
[8] M. Romanelli, C. Leyder, J.-P. Karr, E. Giacobino, and A. Bramati, Phys. Rev. Lett. **98**, 106401 (2007).
[9] C. Leyder, T. C. H. Liew, A. V. Kavokin, I. A. Shelykh, M. Romanelli, J. Ph. Karr, E. Giacobino, and A. Bramati, Phys. Rev. Lett. **99**, 196402 (2007).
[10] I. A. Shelykh, A. V. Kavokin, G. Malpuech, Phys. Status Solidi B **242**, 2271 (2005).
[11] C. Ciuti, V. Savona, C. Piermarocchi, A. Quattropani, and P. Schwendimann, Phys. Rev. B **58**, 7926 (1998).
[12] M. Combescot, O. Betheder-Matibet, and F. Dubin, Phys. Rep. **463**, 215 (2008).
[13] S. Okumura and T. Ogawa, Phys. Rev. B **65**, 035105 (2001).
[14] C. Schindler and R. Zimmermann, Phys. Rev. B **78**, 045313 (2008).
[15] I. A. Shelykh, R. Johne, D. D. Solnyshkov, A. V. Kavokin, N. A. Gippius, and G. Malpuech, Phys. Rev. B **76**, 155308 (2007).
[16] D. N. Krizhanovskii, D. Sanvitto, I. A. Shelykh, M. M. Glazov, G. Malpuech, D. D. Solnyshkov, A. Kavokin, S. Ceccarelli, M. S. Skolnick, and J. S. Roberts, Phys. Rev. B **73**, 073303 (2006).
[17] P. Renucci, T. Amand, X. Marie, P. Senellart, J. Bloch, B. Sermage, and K. V. Kavokin, Phys. Rev. B **72**, 075317 (2005).
[18] J. Kasprzak, R. André, Le Si Dang, I. A. Shelykh, A. V. Kavokin, Yuri G. Rubo, K. V. Kavokin, and G. Malpuech, Phys. Rev. B **75**, 045326 (2007).
[19] I. A. Shelykh, L. Vina, A. V. Kavokin, N. G. Galkin, G. Malpuech, and R. Andre, Solid State Commun. **135**, 1 (2005).
[20] S. Schumacher, N. H. Kwong, and R. Binder, Phys. Rev. B **76**, 245324 (2007).
[21] R. Takayama, N. H. Kwong, I. Rumyantsev, M. Kuwata-Gonokami, and R. Binder, Eur. Phys. J. B **25**, 445 (2002).
[22] M. Combescot, O. Betbeder-Matibet, and R. Combescot, Phys. Rev. B **75**, 174305 (2007).
[23] M. M. Glazov, H. Ouerdane, L. Pilozzi, G. Malpuech, A. V. Kavokin, and A. D'Andrea, arXiv:0902.1410 (unpublished).
[24] A. V. Kavokin and A. I. Nesvizhskii, Phys. Rev. B **49**, 17055 (1994).
[25] A. Kavokin, G. Malpuech, and M. Glazov, Phys. Rev. Lett. **95**, 136601 (2005).
[26] C. Leyder, M. Romanelli, J. Ph. Karr, E. Giacobino, T. C. H. Liew, M. M. Glazov, A. V. Kavokin, G. Malpuech, and A. Bramati, Nat. Phys. **3**, 628 (2007).
[27] The T matrix has been calculated considering the 2D exciton gas implying $V_{\mathrm{dir}} \approx 0$. Its amplitude therefore contains only the information about the exchange and superexchange interaction, depending on the spins [cf. Eqs. (3)–(7)].